processes

MDPI

Article

Coupled Temperature–Pressure Prediction in CO_2 Injection Wells During the Carbon Capture and Storage Process

Ning Liang [1,2,*], Chun-Ai Ma [1,*] and Li Wang [3,4]

[1] School of Economics and Management, China University of Petroleum, Beijing 102249, China
[2] PetroChina Daqing Oilfield Co., Ltd., Daqing 163453, China
[3] Production Technology Research Institute, PetroChina Daqing Oilfield Co., Ltd., Daqing 163712, China; liwang415@163.com
[4] Heilongjiang Province Key Laboratory of Oil and Gas Reservoir Enhanced Production and Injection, Daqing 163453, China
* Correspondence: ningliang2026@163.com (N.L.); mcaxjtu@163.com (C.-A.M.)

Abstract

In carbon capture and storage (CCS) systems, the wellbore serves as a critical connecting channel between CO_2 surface capture facilities and underground storage formations. Accurate prediction of the temperature, pressure, and physical properties of CO_2 fluid within the wellbore is essential for its safe sequestration. In this study, a coupled temperature–pressure-phase prediction model for CO_2 injection wells is established based on the conservation laws of mass, energy, and momentum, combined with the PR-TWU equation of state. The maximum errors in temperature and pressure for the CO_2 injection case well are only 4.57% and 2.05%, respectively, verifying the accuracy of the model. The distribution and variation in temperature, pressure, and physical property parameters in the CO_2 injection wellbore are systematically investigated. The results show that with increasing well depth, the temperature, pressure, and flow velocity of CO_2 fluid exhibit an increasing trend, while its density and viscosity gradually decrease. During CO_2 injection, the well depth at which the CO_2 phase transition occurs is closely related to the critical temperature of CO_2 (31.04 °C). Wellbore pressure is mainly controlled by injection pressure, whereas injection temperature and injection rate are the key parameters affecting wellbore temperature and CO_2 phase transition. The findings can provide a theoretical basis for the optimization of injection parameters and the integrity evaluation of CO_2 sequestration injection wells.

Keywords: CO_2 storage; injection well; temperature and pressure distribution; CO_2 physical property; phase state prediction; injection parameter optimization

Check for updates

Academic Editor: Federica Raganati

Received: 29 December 2025
Revised: 5 February 2026
Accepted: 20 February 2026
Published: 27 February 2026

Copyright: © 2026 by the authors. Licensee MDPI, Basel, Switzerland. This article is an open access article distributed under the terms and conditions of the Creative Commons Attribution (CC BY) license.

1. Introduction

With the increasing severity of global climate change, reducing carbon dioxide (CO_2) emissions has become a critical issue for countries addressing environmental crises. Carbon capture and storage (CCS) technology, as an effective mitigation measure, has gained increasing attention in recent years [1–4]. Among the various components of CCS, the design and management of CO_2 injection wells are key to achieving efficient storage. In practical operations, the temperature and pressure characteristics of injection wells directly affect the CO_2 storage efficiency and its long-term safety [5–8]. Therefore, a systematic study of the coupled temperature and pressure behaviors during the CO_2 injection process is of great significance for optimizing injection practices and ensuring storage safety. The pathways for underground CO_2 sequestration include deep saline

aquifers, basalt formations, unmineable coal seams, and depleted oil and gas reservoirs [9]. During the carbon storage process, CO_2 is injected into deep underground rock formations in a supercritical state, and the temperature and pressure conditions of the formation are altered due to the injection process. According to thermodynamic principles, the injected CO_2 interacts with the surrounding rock, leading to changes in temperature and pressure in localized areas. This coupling effect determines the flow, diffusion, and storage capacity of CO_2. Related studies have shown that accurately predicting the changes in temperature and pressure can not only optimize injection strategies and improve CO_2 storage efficiency but also reduce the potential risk of leakage, ensuring ecological and environmental safety [10,11].

Currently, temperature and pressure in CO_2 injection wells primarily focus on theoretical models. Sun et al. [12] optimized the calculation method for CO_2 thermodynamic properties under supercritical CO_2 drilling wellbore temperature and pressure conditions. Based on the variation laws of CO_2 properties within the wellbore, they established a system of fluid flow control equations for supercritical CO_2 drilling wellbores using the thermodynamic properties of supercritical CO_2 on the flow behavior inside the wellbore. Song et al. [13] considered the effects of axial heat transfer within the wellbore and the temperature changes in the surrounding rock on the flow field. They established a circulation flow model for CO_2 wellbores, enabling the coupled calculation and analysis of pressure parameters, temperature parameters, and CO_2 thermodynamic properties in the flow field. Their study found that the critical depth at which CO_2 in a continuous pipe transitions from liquid to supercritical state was 780 m, and CO_2 in the annulus could always remain in the supercritical state. Li et al. [14] developed a supercritical CO_2 fracturing wellbore flow analytical model based on the Span–Wagner equation of state and the Feng-hour transport property model, combining mass, momentum, and energy conservation equations. By iteratively solving for pressure, temperature, and the interactions between the tubing, annulus, and formation, they achieved dual coupling numerical solutions for both well depth and radial direction. The study revealed that in large-flow supercritical CO_2 fracturing processes, the impact of frictional heat generation on wellbore temperature and pressure should be considered. Wu et al. [15] addressed the temperature and pressure sensitivity of supercritical CO_2 fracturing fluid properties by establishing an unstable pressure field model for supercritical CO_2 fracturing fluid in the pipe–annulus co-injection wellbore, considering the Joule–Thomson effect, axial heat conduction, and wellbore temperature and pressure. They modified the model and obtained the temperature and pressure variation laws of supercritical CO_2 fracturing fluid in the wellbore under co-injection conditions. Yang et al. [16] developed a coupled wellbore CO_2 simulation model with momentum conservation, mass continuity and steady-state heat transfer equations; validated it via field-measured data, identified key influencing factors and provided a practical framework for optimizing injection strategies to boost CO_2 storage capacity and hydrocarbon recovery efficiency. Sang et al. [17] systematically investigated the influence patterns and underlying mechanisms of formation dip angle, CO_2 injection strategy, and their synergistic effects on the CO_2 wellbore leakage process. Cai et al. [18] presented a two-dimensional, transient model to simulate the flow and thermal behavior of CO_2 within a fracturing wellbore. It captured the temporal evolution of temperature, pressure, flow velocity, and fluid density, enabling detailed analysis of phase transitions along different tubing sections.

Although existing studies have explored the temperature, pressure, and flow behavior in CO_2 injection wells to some extent, the effects of CO_2 phase changes and frictional resistance on pressure variation have not been thoroughly investigated. To address this issue, this study develops a comprehensive coupled temperature–pressure phase prediction model for CO_2 injection wells based on the conservation laws of mass, energy, and momen-

tum, combined with the PR-TWU equation of state. The model accounts for the influences of CO_2 density, phase change, frictional resistance, and other factors on temperature and pressure, and systematically investigates the effects of different injection parameters on the wellbore temperature–pressure-phase behavior. The results of this study can provide a theoretical basis for the design and operation of CO_2 sequestration injection wells, injection parameter optimization, and integrity evaluation.

2. Mathematical Model

2.1. Basic Assumptions

During the CO_2 injection process, the CO_2 fluid flows from the surface wellhead to the bottom-hole formation, inducing variations in the temperature and pressure within the wellbore. The flowing CO_2 fluid is subjected to gravitational force, frictional resistance and acceleration pressure drop, which exerts a governing influence on the pressure distribution characteristics in the wellbore. Convective heat exchange of the CO_2 fluid occurs inside the tubing string, and radial heat exchange takes place simultaneously between the CO_2 fluid and the wellbore heat transfer units (including the tubing/casing string, annular protective fluid, cement sheath and formation). A schematic diagram illustrating the flow and heat transfer of CO_2 in the CO_2 injection wellbore is presented in Figure 1.

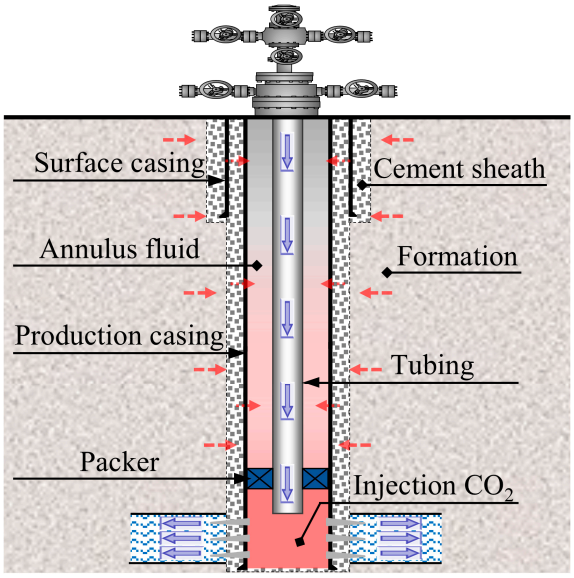


Figure 1. CO_2 flow and heat transfer within the injection wellbore.

To develop a predictive model for the temperature and pressure of CO_2 fluid in injection wellbores, the following assumptions are made for the CO_2 injection process:

(1) The CO_2 fluid in the tubing string is treated as one-dimensional flow;
(2) The axis of the wellbore structure is collinear;
(3) Physical parameters remain uniform across the same cross-section;
(4) Heat transfer in the wellbore is unsteady-state;
(5) The radial heat transfer effect in the wellbore is significantly stronger than the axial one, and the axial heat transfer of the wellbore is neglected.

2.2. CO_2 Physical Property Parameter Model

CO_2 can exist in four states—gaseous, liquid, solid and supercritical states—depending on the variations in temperature and pressure, with its phase diagram shown in Figure 2.

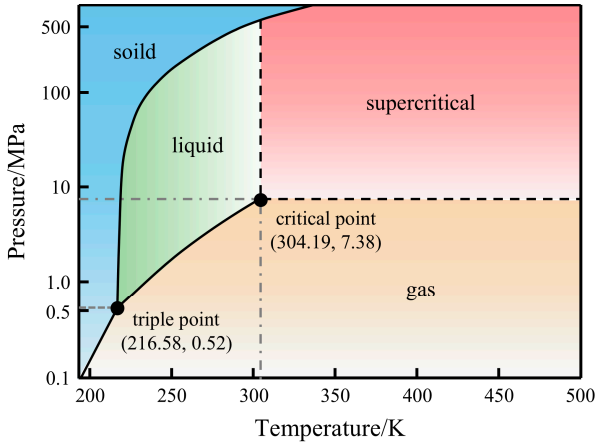


Figure 2. CO_2 phase states.

The thermophysical properties of CO_2 vary significantly with changes in temperature and pressure. For the calculation of CO_2 thermophysical properties, existing methods mainly include the Peng–Robinson (PR) [19], Soave–Redlich–Kwong (SRK) [20], Span–Wagner [21] and Vesovic [22] models, the Fenghour et al. equation [23], and the calculation methods based on Helmholtz free energy, Gibbs free energy and other thermodynamic functions [24]. However, these methods suffer from drawbacks such as large calculation errors or excessive computational complexity. By introducing a temperature correlation function, the PR-TWU equation of state (EOS) significantly improves the accuracy of thermophysical property prediction over a wide temperature range and exhibits excellent precision under high-pressure conditions. It is also capable of accurately predicting the thermophysical properties of CO_2 under near-critical and supercritical conditions, thus meeting the requirements of engineering applications. To accurately characterize the thermophysical properties of CO_2 fluid, this study solves for the density and specific heat capacity of CO_2 based on the PR-TWU EOS, and adopts the Fenghour and Vesovic models to calculate the viscosity and thermal conductivity of CO_2, respectively.

The PR-TWU equation of state is expressed as follows:

$$p = \frac{RT}{V-b} - \frac{a\alpha(T)}{V(V+b)+b(V-b)} \tag{1}$$

where ρ is the density of CO_2 fluid, kg/m^3; R is the gas constant, J/(mol·K); T is the temperature CO_2 fluid, °C; V is the molar volume of CO_2 fluid, in m^3/mol; and $\alpha(T)$, a and b are calculation parameters.

The compressibility factor Z of the PR-TWU equation of state can be expressed as a cubic equation, with its expression given by

$$Z^3 + (B-1)Z^2 + \left(A - 3B^2 - 2B\right)Z + \left(B^3 + B^2 - AB\right) = 0 \tag{2}$$

where Z is the compression factor of the CO_2 fluid, dimensionless; A is the attractive force parameter, dimensionless; and B is a co-volume parameter, dimensionless.

The PR-TWU equation (Equation (2)) can be applied to determine the phase state of CO_2 fluid at a given temperature and pressure. When the real roots of Equation (2) are a single value, three distinct unequal values, and three equal values, the phase states of CO_2 correspond to a single phase (vapor or liquid), a vapor-liquid two-phase, and a supercritical phase, respectively.

$$\rho(T,p) = \frac{pM}{ZRT} \tag{3}$$

where M is the relative molecular mass of the CO_2 fluid, g/mol.

Under low-pressure conditions, the intermolecular interactions of the CO_2 fluid approach zero, and the isobaric specific heat capacity is a function of temperature in this case. The expression for the isobaric specific heat capacity under low-pressure conditions is given by [24]:

$$C_{pi} = B_p + 2C_pT + 3D_pT^2 + 4E_pT^3 + 5F_pT^4 \quad (4)$$

where C_{pi} is the ideal isobaric specific heat capacity under low-pressure conditions, J/(mol·°C); B_p, C_p, D_p, E_p, and F_p are constants.

Under high-pressure conditions, the intermolecular interactions of the CO_2 fluid cannot be neglected. Based on the relationship between the constant-pressure and constant-enthalpy differences and the equation of state, the expression for the residual isobaric specific heat capacity under high-pressure conditions can be derived as follows:

$$\Delta C_p = -RT\left(\frac{\partial^2 \ln\phi}{\partial T^2}\right)_p \quad (5)$$

where $\ln\phi = \frac{b}{V-b} - \frac{a}{2\sqrt{2}bRT}\ln\left(\frac{V+(1-\sqrt{2})b}{V+(1+\sqrt{2})b}\right) + \frac{Z-1}{B} - \ln(Z-B)$; ΔC_p is the residual isobaric specific heat capacity under high-pressure conditions, J/(mol·°C); and ϕ is the fugacity coefficient.

The specific heat capacity of the CO_2 fluid is the sum of the ideal specific heat capacity and the residual specific heat capacity, i.e.,

$$C_p = C_{pi} + \Delta C_p \quad (6)$$

According to the semi-empirical parametric equation derived by Fenghour et al., the viscosity model for CO_2 fluid is given as [23]

$$\mu(T,\rho) = \mu_0(T) + \Delta\mu(T,\rho) + \Delta\mu_c(T,\rho) \quad (7)$$

where μ is the viscosity of the CO_2 fluid, Pa·s; μ_0 is the viscosity value at low pressure, Pa; $\Delta\mu$ is the viscosity increment caused by the increase in density, Pa·s; and $\Delta\mu_c$ is the viscosity increment induced near the critical point, Pa·s.

Based on the semi-empirical parametric equation derived by Vesovic, the thermal conductivity of CO_2 fluid is given by [22]

$$k(T,\rho) = k_0(T) + \Delta k(T,\rho) + \Delta k_c(T,\rho) \quad (8)$$

where k is the thermal conductivity of CO_2 fluid, W/(m·°C); k_0 is the thermal conductivity at low pressure, W/(m·°C); Δk is the increase in thermal conductivity caused by the rise in density, W/(m·°C); and Δk_c is the increase in thermal conductivity induced by the vicinity of the critical point, W/(m·°C).

2.3. CO_2 Temperature Field Model

During the CO_2 injection process, heat exchange occurs in both radial and axial directions between the CO_2 and the wellbore components, including the tubing, annular fluid, cement sheath, and surrounding formation. Based on the principle of energy conservation, and considering the fluid heat content Q, internal energy E_{in}, transferred heat E_{ab}, and

mechanical energy E_{me}, the energy conservation equation for the CO_2 elemental fluid within a differential time interval dt and a wellbore segment dz can be expressed as

$$dQ = \frac{dE_{in}}{dt} + \frac{dE_{ab}}{dt} - \frac{dE_{me}}{dz} \tag{9}$$

According to the fundamental assumption of one-dimensional radial unsteady-state heat conduction, the radial heat transfer in the wellbore is governed by the following differential equation:

$$\frac{\partial^2 T}{\partial r^2} + \frac{1}{r}\frac{\partial T}{\partial r} = \frac{1}{\alpha}\frac{\partial T}{\partial t} \tag{10}$$

where T represents the wellbore temperature, °C; r represents the radius of the wellbore, m; and α is the thermal diffusivity coefficient, s/m^2.

Equation (9) is solved using the method proposed by Hasan [25], leading to the temperature equation of the CO_2 fluid inside the wellbore:

$$\frac{dT_f}{dt} = \frac{w}{m(1+C_T)}\left[L_R\left(T_f - T_{ei}\right) + \frac{\partial T_f}{\partial z} + \phi - \frac{g\cos\theta}{c_p}\right] \tag{11}$$

where

$$\phi = g_G\cos\theta + \frac{v}{c_p}\frac{dv}{dz} - C_J\frac{dp}{dz},\ L_R = \frac{2\pi}{wc_p}\left(\frac{r_{so}U_t k_e}{\lambda_e + r_{so}U_t T_D}\right)$$

where T_f represents the temperature of the CO_2 fluid, °C; w represents the mass flow rate of the CO_2 fluid, in kg/s; m represents the mass of CO_2 fluid per unit length in the wellbore, kg/m; C_T is the heat storage coefficient, dimensionless; L_R is the relaxation distance, m; T_{ei} stands for formation temperature, °C; ϕ is an intermediate variable, °C/m; g is the acceleration due to gravity, m/s^2; θ is the well inclination angle, °; c_p is the specific heat capacity at constant pressure of the CO_2 fluid, J/(kg·°C); g_G represents the geothermal gradient, °C/m; v represents the flow velocity of the CO_2 fluid, in m/s; C_J is the Joule–Thomson coefficient, °C/Pa; r_{so} is the outer radius of the CO_2 injection pipe string, m; U_t is the overall heat transfer coefficient, W/(m^2·°C); k_e is the thermal conductivity of the formation, W/(m·°C); and T_D is a dimensionless time function.

Integrating Equation (10), the analytical solution for the temperature distribution of the CO_2 fluid in the wellbore is obtained as

$$T_f = T_{ei} - \frac{\phi}{L_R}\left[1 - e^{\frac{wtL_R}{m(1+C_T)}}\right]\left[1 - e^{(z-L)L_R}\right] \tag{12}$$

where L represents the depth of the wellbore, m.

2.4. CO_2 Pressure Field Model

The pressure of CO_2 within the wellbore is influenced by its temperature and thermophysical properties. Based on the law of mass conservation, the continuity equation for an elemental control volume of CO_2 fluid in the wellbore is expressed as

$$\rho\frac{dv}{dz} + v\frac{dp}{dz} = 0 \tag{13}$$

According to the principle of momentum conservation, the rate of momentum change in the elemental CO_2 fluid is equal to the resultant external forces acting upon it. The

primary forces include gravitational force, frictional resistance, and acceleration-induced pressure drop. Therefore, the total pressure gradient of the CO_2 fluid can be expressed as

$$\frac{dp}{dz} = \rho g \cos\theta + \rho f \frac{v^2}{4r_{si}} + \rho v \frac{dv}{dz} \tag{14}$$

where f is the friction coefficient, dimensionless; r_{si} is the inner radius of the CO_2 injection string, m.

The friction coefficient in Equation (6) is calculated by

$$f = \left[1.14 - 2\lg\left(\frac{\varepsilon}{2r_{si}} + \frac{21.25}{Re^{0.9}}\right)\right]^{-2} \tag{15}$$

where ε represents the absolute roughness of the CO_2 injection pipe wall, dimensionless; Re is the Reynolds number, and is dimensionless.

Based on the established coupling model for CO_2 physical properties, temperature, and pressure fields, iterative calculations are performed using a self-developed Python 3.14 program following the procedure of initial value determination, model substitution, result comparison and accuracy verification. The model calculation flowchart is shown in Figure 3. The computations are conducted on a workstation equipped with an Intel i7-13700 K (16-core) CPU and 32 GB of RAM, with an average computational time of 27.47 s for a single simulation run.

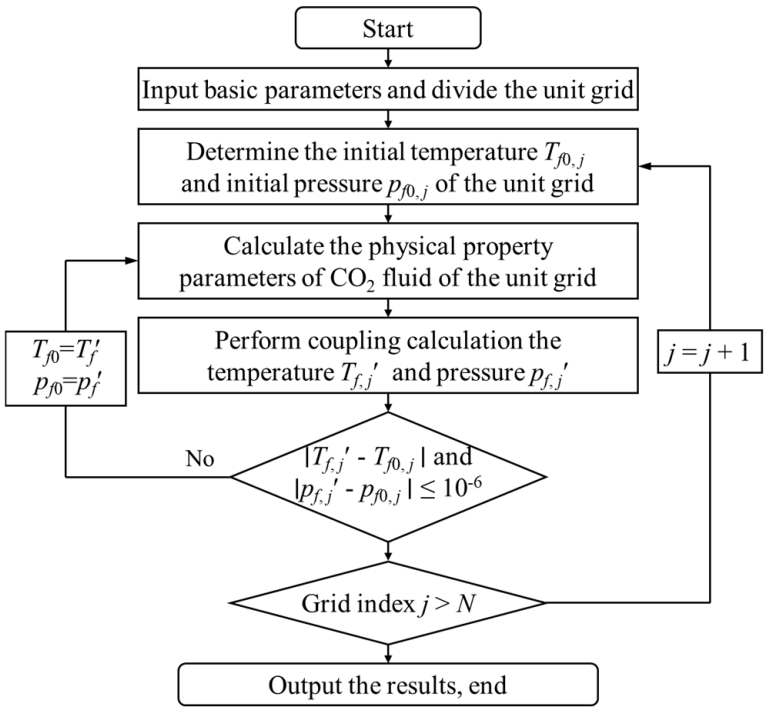


Figure 3. Model calculation flowchart.

3. Field Case Validation

3.1. Basic Data

Taking a CO_2 injection well (S-well) in D Oilfield in China as an example, this study investigates the distribution characteristics of temperature, pressure and thermophysical properties of CO_2 along the wellbore during the injection operation. The basic data used for the calculations are summarized in Table 1.

Table 1. Basic data of the S-well.

Parameter	Unit	Value
Outer diameter of the casing	mm	139.70
Wall thickness of the casing	mm	7.72
Depth of the casing	m	2176.0
Outer diameter of the cement sheath	mm	234.50
Cement top depth	m	1428.0
Outer diameter of the tubing	mm	73.02
Wall thickness of the tubing	mm	5.51
Depth under the tubing	m	2100.0
Packer depth	m	1920
Formation pressure	MPa	22.6
Formation temperature	°C	75.0
Thermal conductivity of formation	$W\cdot(m^{-1}\cdot°C^{-1})$	2.0
Thermal diffusion coefficient of formation	$m^2\cdot h^{-1}$	0.0037
Thermal conductivity of the cement sheath	$W\cdot(m^{-1}\cdot°C^{-1})$	0.75
Radiation heat transfer coefficient in the annular	$W\cdot(m^{-2}\cdot°C^{-1})$	5.0
Convective heat transfer coefficient in the annular	$W\cdot(m^{-2}\cdot°C^{-1})$	6.0
Thermal conductivity of the string	$W\cdot(m^{-1}\cdot°C^{-1})$	45.0
Injection temperature	°C	0.0
Injection pressure	MPa	26.0
Injection time	*d*	100.0
Injection rate	$t\cdot d^{-1}$	40.0

3.2. Model Verification

A comparison between the field-measured data and the model predictions is presented in Figure 4. As shown in Figure 4, the maximum relative errors in the predicted temperature and pressure along the CO_2 injection well are 4.57% and 2.05%, respectively. The accuracy and applicability of the model proposed in this paper have been verified.

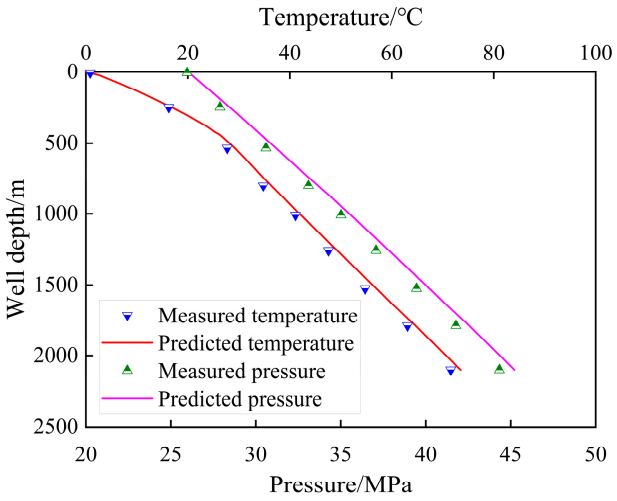
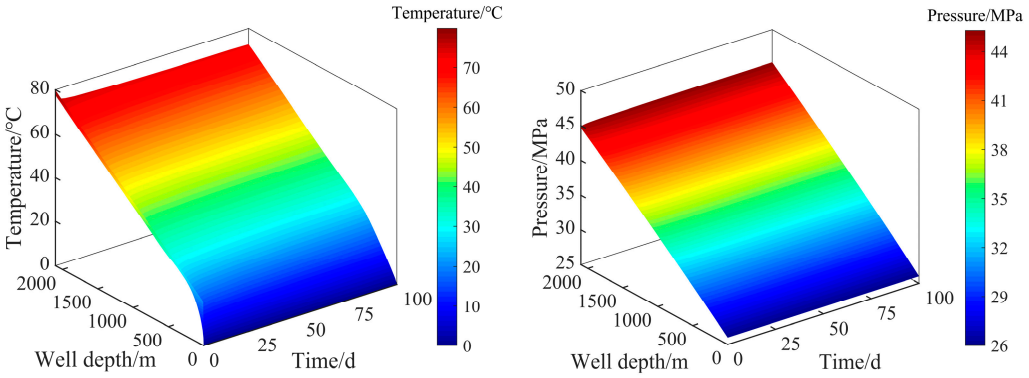


Figure 4. Comparison results of model verification.

3.3. Result Analysis

The wellbore temperature and pressure profiles of the CO_2 injection well are presented in Figure 5. As can be seen from Figure 5a, at short injection times, the wellbore temperature decreases due to the effect of the injection temperature difference; with the increase in injection time, the radial heat exchange in the wellbore gradually stabilizes, and the wellbore temperature also tends to be stable. This is because the CO_2 fluid exchanges heat with the

wellbore and formation under the influence of injection time, and the heat exchange rate gradually stabilizes with increasing injection time. The wellbore temperature distribution basically reaches a steady state at an injection time of 30 days. It can be observed from Figure 5b that the wellbore pressure increases linearly with the increase in well depth, which is attributed to the fact that the gravity of the injected CO_2 fluid dominates over the frictional pressure. Injection time has a negligible effect on wellbore pressure. With the increase in injection time, the decrease in wellbore temperature leads to a slight rise in bottom-hole pressure, the mechanism of which is that the temperature drop reduces the density of CO_2 in the wellbore. A comparison of Figure 5a,b shows that pressure reaches a steady state much faster than temperature; although temperature variation alters the physical property parameters of CO_2 in the wellbore, such variation exerts a minor influence on wellbore pressure.



(**a**) Temperature (**b**) Pressure

Figure 5. Temperature and pressure profile of CO_2 injection well.

The variation patterns of physical properties of CO_2 fluid, including flow velocity, density, viscosity and phase state, are depicted in Figure 6. As shown in Figure 6a, the flow velocity increases gradually with increasing well depth; at short injection times, the fluctuation of flow velocity at the same well depth is induced by the disturbance from the unstable temperature field. The flow velocity of CO_2 fluid ranges from 0.146 to 0.179 m/s. It can be seen from Figure 6b that the density decreases progressively with the increase in well depth; with the extension of injection time, the density at the same well depth rises rapidly at first and then gradually approaches a steady state, with the overall density range of CO_2 fluid being 851 to 1042 kg/m^3. As illustrated in Figure 6c, the viscosity shows a gradual decrease with increasing well depth; similarly, the viscosity at the same well depth increases rapidly initially and then stabilizes gradually with prolonged injection time, and the viscosity of the CO_2 fluid varies from 0.087 to 0.142 mPa·s. It is indicated in Figure 6d that with the increase in injection time, the well depth at which CO_2 fluid transforms from the liquid phase to the supercritical phase increases rapidly at first and then rises slowly until it stabilizes gradually. The phase state of CO_2 fluid is governed by temperature and pressure conditions, and the well depth for its phase transition ranges from 560 to 870 m, a mechanism that is closely associated with the critical temperature of CO_2 (31.04 °C). With the increase in injection time, the critical well depth for the phase transition of CO_2 fluid increases by 55.4%.

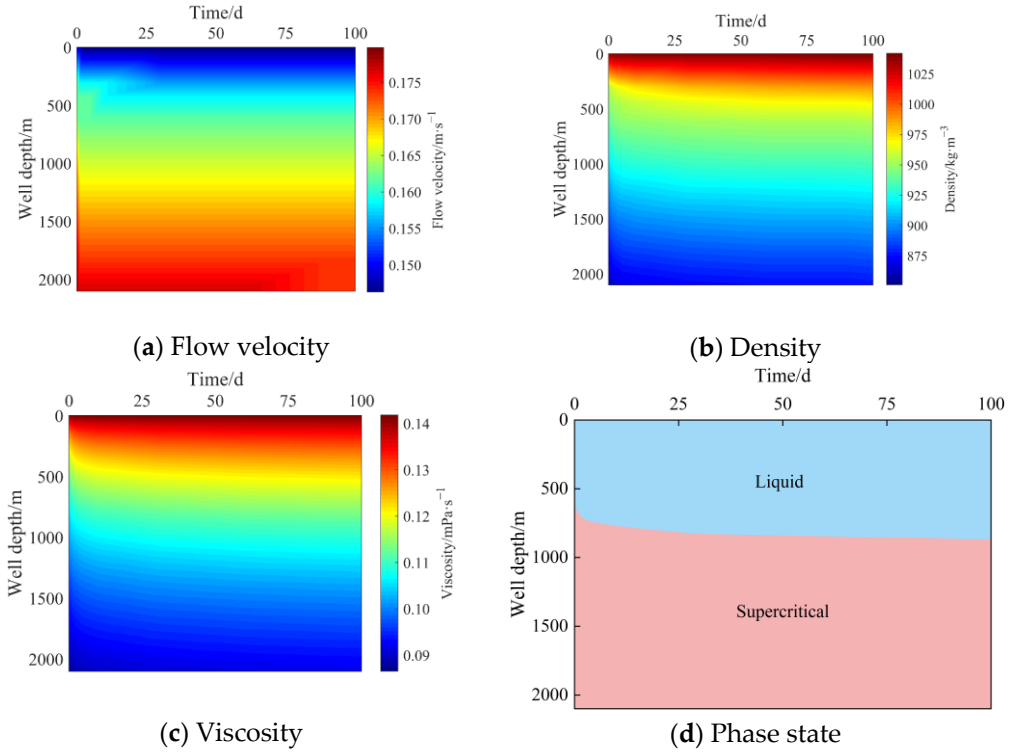


Figure 6. Physical property parameters of CO_2 fluid.

3.4. Sensitivity Analysis

To investigate the impact of varying CO_2 injection parameters, a fixed injection duration of 30 days was employed. The effects of different injection temperatures, injection pressures, and injection rates on the variations in wellbore temperature, pressure, and phase behavior were systematically analyzed.

3.4.1. Effect of Injection Temperature

The variation law of wellbore temperature under different injection temperatures is illustrated in Figure 7. As can be seen from the figure, the temperature inside the tubing decreases with the reduction in CO_2 injection temperature, indicating a significant effect of CO_2 injection temperature on wellbore temperature. At the bottom-hole position, the maximum increase in wellbore temperature under different CO_2 injection temperatures reaches 1.60 °C. Owing to the temperature difference between the injection fluid and the formation, the temperature inside the tubing rises markedly at a well depth ranging from 0 to approximately 450 m, where radial heat exchange dominates the heat transfer process. In the depth interval from 450 m to the bottom of the well, the temperature inside the tubing exhibits a linear increasing trend; here, the temperature difference between the fluid and the formation is small, and axial heat exchange becomes the dominant mode. The temperature increment becomes progressively weaker with increasing well depth, which is attributed to the decreasing temperature difference between the injected CO_2 and the formation, leading to a reduction in the heat exchange rate.

The variation law of wellbore pressure under different injection temperatures is illustrated in Figure 8. It can be seen from Figure 8 that the pressure in the tubing string increases linearly with the increase in well depth. At the bottom-hole position, the maximum reduction in wellbore pressure is merely 0.23 MPa under different CO_2 injection temperatures. The density of CO_2 decreases under high-temperature conditions, which in turn leads to a reduction in bottom-hole pressure. Since the effect of different CO_2 injection

temperatures on the CO_2 density in the wellbore is slight, their influence on the wellbore pressure is also negligible.

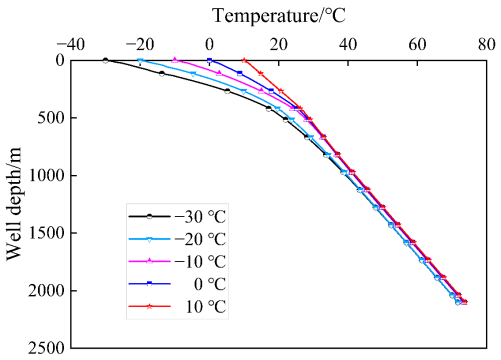


Figure 7. Wellbore temperature variation under different injection temperatures.

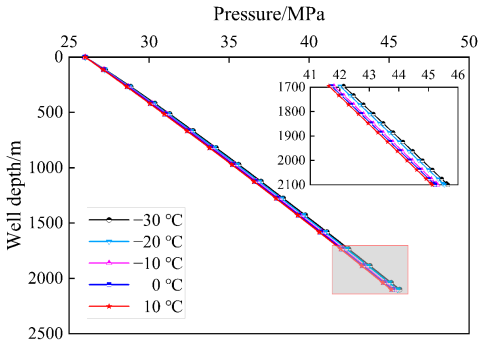


Figure 8. Wellbore pressure variation under different injection temperatures.

The phase distribution law of CO_2 under different injection temperatures is illustrated in Figure 9. It can be seen from Figure 9 that with the decrease in injection temperature, the well depth at which the CO_2 fluid transitions from the liquid phase to the supercritical phase decreases accordingly. Owing to the combined effects of temperature and pressure conditions, the well depth for the phase transition of CO_2 fluid reduces from 890 m to 790 m, with a reduction amplitude of 11.2%. Since different injection temperatures exert only a minor influence on the wellbore temperature and pressure, their impact on the CO_2 phase state is also insignificant.

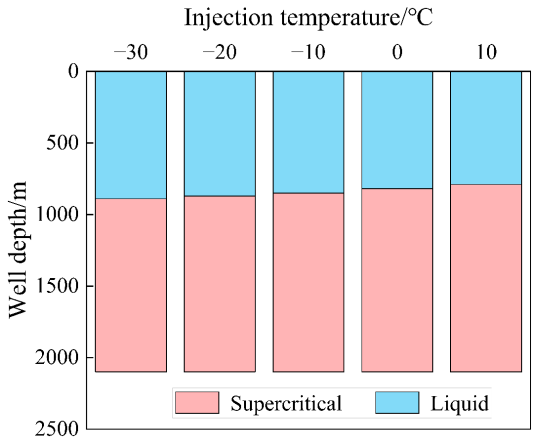


Figure 9. Phase distribution of CO_2 under different injection temperatures.

3.4.2. Effect of Injection Pressure

The variation law of wellbore temperature under different injection pressures is illustrated in Figure 10. It can be seen from Figure 10 that an increase in injection pressure only causes a slight decrease in bottom-hole temperature, and its influence on wellbore temperature is extremely minor. At the bottom-hole position, the maximum reduction in wellbore temperature is merely 0.16 °C under different CO_2 injection pressures. Although the flow velocity of CO_2 fluid increases under high-pressure conditions, which shortens the heat exchange time, the injection rate of 30 t/d is relatively low in this case, and the effect of pressure on the thermophysical parameters related to CO_2 heat transfer is also negligible. For these reasons, the influence of injection pressure on wellbore temperature is extremely small.

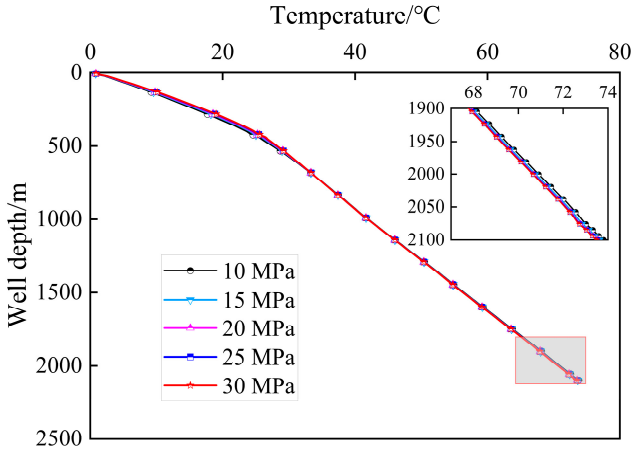


Figure 10. Wellbore temperature variation under different injection pressures.

The variation law of wellbore pressure under different injection pressures is illustrated in Figure 11. It can be seen from Figure 11 that the wellbore pressure increases significantly with the rise in injection pressure, indicating a remarkable influence of injection pressure on wellbore pressure. At the bottom-hole position, the maximum increase in wellbore pressure reaches 5.96 MPa with the increase in injection pressure, corresponding to an increase in amplitude of 84.2%. Owing to the low CO_2 injection rate, the pressure gradient is slightly affected by the injection pressure. The increase in CO_2 density under high-pressure conditions will raise the hydrostatic column pressure of the CO_2 fluid, meaning that adjusting the injection pressure can effectively enhance the bottom-hole pressure.

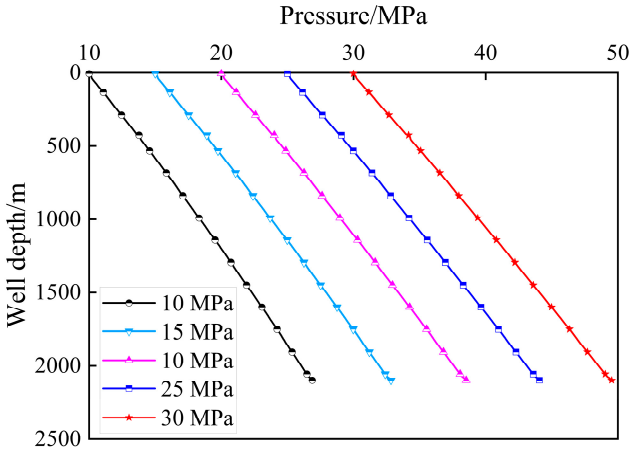


Figure 11. Wellbore pressure variation under different injection pressures.

The phase distribution law of CO_2 under different injection pressures is illustrated in Figure 12. It can be seen from Figure 12 that with the increase in injection pressure, the well depth at which the CO_2 fluid undergoes phase transition increases slightly at first and then decreases marginally. This phenomenon is mainly caused by the variation in the well depth corresponding to the critical temperature of CO_2 (31.04 °C) in the wellbore under different injection pressures. Under different injection pressures, the maximum variation amplitude of the well depth for the CO_2 fluid phase transition is 6.2%. Since the injection pressure exceeds the critical pressure of the CO_2 fluid, its influence on the CO_2 phase state is minor.

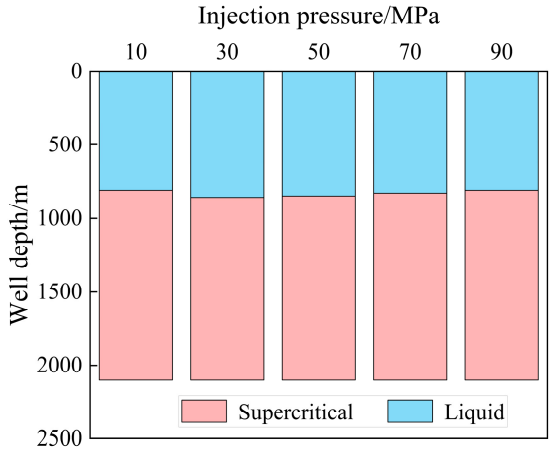


Figure 12. Phase distribution of CO_2 under different injection pressures.

3.4.3. Effect of Injection Rate

The variation law of wellbore temperature under different injection rates is illustrated in Figure 13. It can be seen from Figure 13 that the CO_2 injection rate exerts an extremely significant influence on the wellbore temperature, and the temperature in the tubing string decreases gradually with the increase in the CO_2 injection rate. This is mainly because under the condition of a high injection rate, the high flow velocity shortens the time for convective heat transfer between the CO_2 fluid and the tubing string and heat conduction in the wellbore; accordingly, the heat loss is lower, leading to a lower wellbore temperature. At the bottom-hole position, the maximum reduction in wellbore temperature reaches 2.90 °C under different CO_2 injection rates.

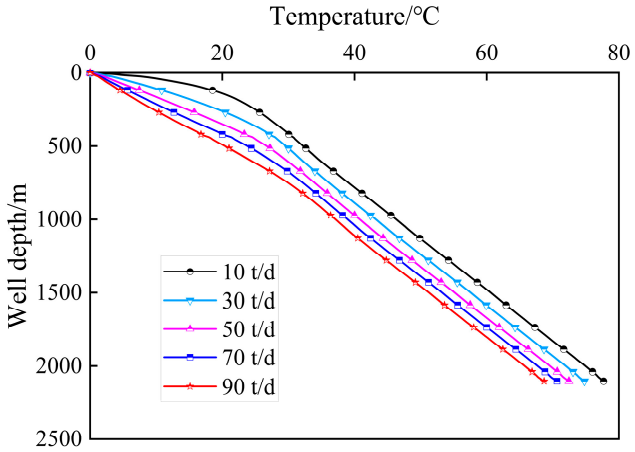


Figure 13. Wellbore temperature variation under different injection rates.

The variation law of wellbore pressure under different injection rates is illustrated in Figure 14. It can be seen from Figure 14 that the bottom-hole pressure decreases gradually

with the increase in the CO_2 injection rate. Under the condition of a high injection rate, the temperature of the CO_2 fluid is lower, and the reduction in its density will lead to a decrease in hydrostatic pressure; meanwhile, a high injection rate will increase the frictional pressure loss, resulting in a lower bottom-hole pressure when these effects are superimposed. At the bottom-hole position, the maximum increase in wellbore pressure is merely 0.26 MPa under different CO_2 injection rates. Thus, the CO_2 injection rate exerts a minor influence on the wellbore pressure.

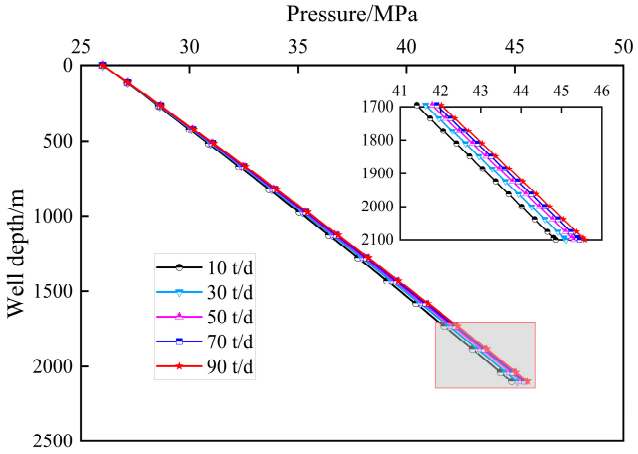


Figure 14. Wellbore pressure variation under different injection rates.

The phase distribution law of CO_2 under different injection rates is illustrated in Figure 15. It can be seen from Figure 15 that the well depth at which the CO_2 fluid undergoes phase transition increases gradually with the rise in the CO_2 injection rate. This phenomenon stems from the variation in the well depth corresponding to the critical temperature of CO_2 (31.04 °C) in the wellbore under the condition of a high injection rate. The well depth for the CO_2 fluid phase transition increases from 500 m to 1210 m, with an increase in amplitude of 142.0%. The CO_2 injection rate exerts a remarkable influence on the CO_2 phase state, which is attributed to the significant effect of the injection rate on the wellbore temperature.

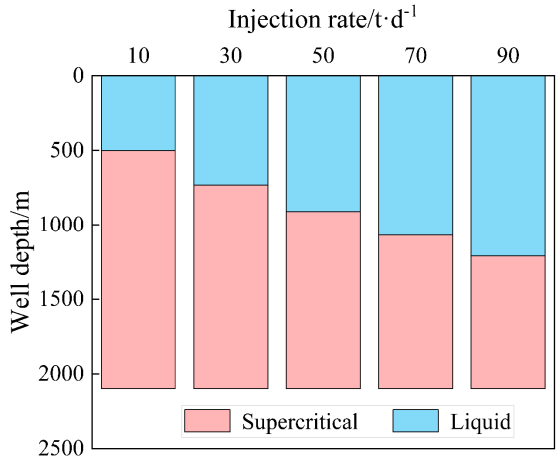


Figure 15. Phase distribution of CO_2 under different injection rates.

The effects of different injection parameters on wellbore temperature, pressure and CO_2 phase state are analyzed and summarized in Table 2. It can be seen from Table 2 that the order of the influence degree of different injection parameters on wellbore temperature from the highest to the lowest is as follows: injection temperature, injection pressure, injection

rate. For wellbore pressure, the order of influence degree from the highest to the lowest is: injection pressure, injection rate, injection temperature. As for the CO_2 phase state, the order of influence degree from the highest to the lowest is: injection rate, injection pressure, injection temperature. In the optimization of CO_2 injection parameters, it is recommended to optimize the injection temperature and injection rate for wellbore temperature regulation; optimize the injection pressure alone for wellbore pressure adjustment; and optimize the injection rate and injection temperature for CO_2 phase state control.

Table 2. Analysis of the influence of different injection parameters.

Influencing Parameters	Change in Influence Parameter	Bottom-Hole Temperature Change	Bottom-Hole Pressure Change	Phase Transition Well Depth
Injection temperature	Increase by 10 °C	Maximum increase of 1.60 °C	Maximum decrease of 0.23 MPa	Maximum decrease of 30 m
Injection pressure	Increase by 5 MPa	Maximum decrease of 0.16 °C	Maximum increase of 5.96 MPa	Maximum increase of 50 m, Maximum decrease of 20 m
Injection rate	Increase by 20 t/d	Maximum decrease of 2.90 °C	Maximum increase of 0.26 MPa	Maximum increase of 230 m

4. Conclusions

(1) Based on the conservation laws of mass, energy and momentum for CO_2 fluid, a coupled prediction model for wellbore temperature–pressure-phase state of CO_2 injection wells was established in combination with the PR-TWU phase equilibrium equation. A comparison between the field-measured and predicted results of CO_2 injection wells shows that the maximum relative errors of temperature and pressure are 4.57% and 2.05%, respectively, which verifies the accuracy of the proposed model in this study.

(2) During the CO_2 injection process, the temperature, pressure and flow velocity of CO_2 fluid in the wellbore increase with the rise in well depth, while the density and viscosity decrease accordingly. With the increase in injection time, in contrast to the wellbore pressure reaching a steady state instantaneously, the wellbore temperature and the well depth of the CO_2 fluid phase transition decrease rapidly at first and then gradually tend to be stable.

(3) The wellbore pressure is mainly regulated by the injection pressure, while the injection temperature and injection rate are the key parameters affecting the wellbore temperature and CO_2 phase transition. The phase transition of CO_2 at the critical temperature of 31.04 °C is the key reason for the variation in the well depth of phase transition in CO_2 injection wells.

(4) This study investigates the coupled distribution laws of temperature, pressure, phase state and other parameters of CO_2 in the injection wellbore for carbon capture and storage (CCS). However, the effects of unsteady heat transfer and impure CO_2 flow conditions are not involved. It is recommended that further in-depth research be conducted in subsequent studies.

Author Contributions: Conceptualization, methodology, software, writing—original draft preparation, and funding acquisition, N.L.; validation, formal analysis, and investigation, L.W.; resources, writing—review and editing, and supervision, C.-A.M. All authors have read and agreed to the published version of the manuscript.

Funding: This research was funded by the China National Petroleum Corporation Major Scientific and Technological Project, grant number 2021ZZ01.

Data Availability Statement: The original contributions presented in this study are included in the article. Further inquiries can be directed to the corresponding authors.

Acknowledgments: This work was supported by the China National Petroleum Corporation Major Scientific and Technological Project (2021ZZ01).

Conflicts of Interest: Author Ning Liang was employed by the PetroChina Daqing Oilfield Co., Ltd.; Author Li Wang was employed by the Production Technology Research Institute, PetroChina Daqing Oilfield Co., Ltd. The remaining authors declare that the research was conducted in the absence of any commercial or financial relationships that could be construed as a potential conflict of interest. The China National Petroleum Corporation Major Scientific and Technological Project grant number [2021ZZ01] had no role in the design of the study; in the collection, analyses, or interpretation of data; in the writing of the manuscript; or in the decision to publish the results.

References

1. Shao, T.M.; Pan, X.Z.; Wang, L.N.; Xiong, W.; Wang, T.; Song, J. Assessing CCS development uncertainties in China's energy system aligned with carbon neutrality. *Appl. Energy* **2025**, *299*, 126545. [CrossRef]
2. Chen, S.Y.; Liu, J.F.; Zhang, Q.; Teng, F.; McLellan, B.C. A critical review on deployment planning and risk analysis of carbon capture, utilization, and storage (CCUS) toward carbon neutrality. *Renew. Sustain. Energy Rev.* **2022**, *167*, 112537. [CrossRef]
3. Mitterrutzner, B.; Sovacool, B.K.; Knudsen, B.; Bazilian, M.D.; Kim, J.; Roussanaly, S.; Tomasgard, A.; Griffiths, S. Scaling carbon capture and storage (CCS) to gigaton capacity: A multi-dimensional and critical review. *Int. J. Greenh. Gas Control* **2026**, *149*, 104531. [CrossRef]
4. Kang, N.; Sarsenbekuly, B.; Wu, H.R. Progress of CCUS technology with enhanced oil recovery. *J. CO_2 Util.* **2025**, *102*, 103233. [CrossRef]
5. Li, H.; Li, J.; Lian, W.; Zhang, H.; Liu, J. Wellbore thermo-mechanical response during CO_2 mixture geological sequestration in depleted reservoirs. *Geoenergy Sci. Eng.* **2026**, *257*, 214244. [CrossRef]
6. Yang, Z.H.; Cheng, J.R.; Li, Z.F.; Yang, Y.; Tang, L.; Wei, W. Unsteady flow dynamics and phase transition behavior of CO_2 in fracturing wellbores. *Fluid Dyn. Mater. Process.* **2025**, *21*, 2149–2176. [CrossRef]
7. Li, Q.; Wang, D.; Zhang, H.; Li, J.; Lian, W.; Yang, H.; Jiang, B. Study on the stress-corrosion failure of tubing in CO_2-EOR wellbores. *Eng. Fail. Anal.* **2026**, *185*, 110369. [CrossRef]
8. Gao, X.Y.; Yang, S.L.; Wang, B.D.; Shen, B.; Zhao, E.; Rui, Z. Wellbore-reservoir and multiphysics coupling model for liquid CO_2 cyclic injection in a CCUS-EGR framework. *J. Hydrol.* **2025**, *658*, 133188. [CrossRef]
9. Dumitrache, L.; Suditu, S.; Branoiu, G.; Neagu, D.; Alecu, M.D. Carbon Management and Storage for Oltenia: Tackling Romania's Decarbonization Goals. *Sustainability* **2025**, *17*, 6793. [CrossRef]
10. Zhang, F.Y.; Cao, W.X.; Lu, R.H.; Rui, Z.; Babadagli, T.; Xia, Q.; Ji, Z. Multiphase flow model of CO_2 and formation fluid for production wellbores in CO_2 geological storage. *Fuel* **2026**, *410*, 137903. [CrossRef]
11. He, Y.M.; Song, L.; Ranjith, P.G.; Huang, M.; Sun, Y.; Wang, Z.; Wu, L. Evolution of resistivity and permeability of wellbore cement after corrosion by supercritical CO_2 in geological CO_2 storage conditions. *Constr. Build. Mater.* **2025**, *473*, 141015. [CrossRef]
12. Sun, B.J.; Sun, X.H.; Wang, Z.Y.; Liu, S.J.; Xia, Q.; Cai, D.J. Flow behavior analysis during supercritical CO_2 drilling: Consideration of varying thermo-physical properties of CO_2 in wellbore. *J. China Univ. Pet.* **2016**, *40*, 88–95.
13. Song, W.Q.; Ni, H.J.; Jing, Y.H.; Wang, R.; Shen, Z.; Li, B. Study on wellbore flow field of supercritical carbon dioxide drilling. *J. China Univ. Pet.* **2017**, *41*, 101–107.
14. Li, X.J.; Li, G.S.; Wang, H.Z.; Tian, S.Z.; Song, X.Z.; Lu, P.Q.; Liu, Q.L. A wellbore flow model and coupling solution for supercritical CO_2 fracturing. *J. China Univ. Pet.* **2018**, *42*, 87–94.
15. Wu, L.; Luo, Z.F.; Zhao, L.Q.; Zhang, N.; Yao, Z.; Jia, Y. Transient temperature-pressure field model of supercritical CO_2 fracturing wellbore with tubing and annulus co-injection. *Greenh. Gases Sci. Technol.* **2022**, *12*, 85–102. [CrossRef]
16. Yang, Z.; Yan, W.; Lv, W.; Tang, Q.; Duan, J.; Li, M.; Zhou, P.; Li, J.; Yang, T. Study on the phase state and temperature-pressure distribution of CO_2 injection wellbore and its effect on tubing stress conditions. *Geoenergy Sci. Eng.* **2024**, *241*, 213155. [CrossRef]
17. Sang, Y.; Du, A.; Ye, C.; Xiang, J.; Chen, Y.; Guo, Y.; Shen, L. Temperature and pressure profiles during prolonged working fluid injection in wellbores: Mechanisms and key influencing factors. *Fluid Dyn. Mater. Process.* **2025**, *21*, 1623–1639. [CrossRef]
18. Cai, Y.; Yang, D.; Lei, H.; Feng, G. Influence of formation dip angle and injection strategy on CO_2 wellbore leakage with consideration of CO_2 transient flow and phase transition. *Energy* **2025**, *330*, 136889. [CrossRef]
19. Pan, L.H.; Oldenburg, C.M.; Wu, Y.S.; Pruess, K. Wellbore flow model for carbon dioxide and brine. *Energy Procedia* **2009**, *1*, 71–78. [CrossRef]
20. Soave, G. Rigorous and simplified procedures for determining the pure-component parameters in the Redlich-Kwong-soave equation of state. *Chem. Eng. Sci.* **1980**, *35*, 1725–1730. [CrossRef]
21. Span, R.; Wagner, W. A new equation of state for carbon dioxide covering the fluid region from the triple-point temperature to 1100 K at pressures up to 800 MPa. *J. Phys. Chem. Ref. Data* **1996**, *25*, 1509–1596. [CrossRef]
22. Vesovic, V.; Wakeham, W.A.; Olchowy, G.A.; Sengers, J.V.; Watson, J.T.R.; Millat, J. The transport properties of carbon dioxide. *J. Phys. Chem. Ref. Data* **1990**, *19*, 763–808. [CrossRef]

23. Fenghour, A.; Wakeham, W.A.; Vesovic, V. The viscosity of carbon dioxide. *J. Phys. Chem. Ref. Data* **1998**, *27*, 31–44. [CrossRef]
24. Lemmon, E.W.; Tillner-Roth, R. A Helmholtz energy equation of state for calculating the thermodynamic properties of fluid mixtures. *Fluid Phase Equilibria* **1999**, *165*, 1–21. [CrossRef]
25. Hasan, A.R.; Kabir, C.S. Wellbore heat-transfer modeling and applications. *J. Pet. Sci. Eng.* **2012**, *86*, 127–136. [CrossRef]

Disclaimer/Publisher's Note: The statements, opinions and data contained in all publications are solely those of the individual author(s) and contributor(s) and not of MDPI and/or the editor(s). MDPI and/or the editor(s) disclaim responsibility for any injury to people or property resulting from any ideas, methods, instructions or products referred to in the content.